

Visualizing the velocity fields and fluid behavior of a solution using artificial intelligence during EndoActivator activation

Harry Huiz Peeters¹, Elvira Theola Judith², Faber Yosua Silitonga³, Lavi Rizki Zuhul³

¹Laser Research Center in Dentistry, Bandung, Indonesia

²Faculty of Dentistry, Universitas Maranatha, Bandung, Indonesia

³Faculty of Mechanical and Aerospace Engineering, Institut Teknologi Bandung, Bandung, Indonesia

ABSTRACT

Background: Electrical devices driven sonically have been found in several studies to be effective to clean root canals but the effect of the EndoActivator irrigant activation flow behavior on cleaning efficacy is not completely understood. **Purpose:** The study aimed to provide an initial understanding of flow behavior and velocity field generation during the irrigant activation process by EndoActivator using artificial intelligence (AI). **Methods:** A straight glass model was filled with a solution containing 17% EDTA. Meanwhile, a medium activator tip with 22-mm polymer noncutting #25, 0.04 file driven by an electrical sonic hand-piece at 190 Hz (highest level) was used to induce velocity field to produce micro-bubbles. The physical mechanisms involved were recorded using a Miro 320S high-speed imaging system, the hydrodynamic responses were recorded, and analyzed using a motion estimation program supported by LiteFlowNet (AI). **Results:** The rapid fluid flow was visualized clearly in the model when it was activated by an EndoActivator tip. It was also observed that the distal end of the EndoActivator tip generated a near-wall high gradient velocity apically in all directions of the oscillation. **Conclusion:** The analysis showed that the proposed motion estimation program, supported by LiteFlowNet (AI), was able to capture velocity magnitude estimation of a non-PIV experiment and visualize the bubbles generated in the solution.

Keywords: artificial intelligence; EndoActivator; endodontics; natural frequency; shear stress

Correspondence: Harry Huiz Peeters, Laser Research Center in Dentistry, Cihampelas 41 Bandung, West Java, 40174, Indonesia.
Email: h2huiz@cbn.net.id

INTRODUCTION

A pre-requisite to the long-term success of root canal treatment is the thorough debridement and disinfection of the root canal system.^{1–4} Meanwhile, the efficacy of an irrigation delivery or agitation system to debride depends on how the irrigant reaches the apical region, the un-instrumented areas, and the ability to create a strong current enough to carry the debris out of the root canal coronally.^{5–9} Some examples of machine-assisted agitation are electrical ultrasonic and sonic devices¹⁰ that use a fine non-cutting polymer or metal tip vibrated within the root canal space at different frequencies based on the manufacturer's instruction. It is important to note that sonically activated instruments utilize frequencies in the range of 1,000–6,000 Hz and generate a single node near the point at which the file is attached and an antinode at the tip of the file.^{11–13}

EndoActivator (Dentsply, Tulsa Dental) was introduced onto the market and has been developed with the intention of activating root canal irrigants by energizing the solution with sonic energy. Several controversial results have been reported but sonically driven electrical devices have been found in different studies to be effective in cleaning root canals.^{12,14,15}

Powerful particle image velocimetry (PIV) technology has also been used in several studies on dentistry to observe the natural flow behavior of hydrodynamic response during irrigation activation.^{16–19} A deep learning approach for motion estimation currently showed promising results with higher accuracy and enhanced computational performance.²⁰ Moreover, the LiteFlowNet network which is a state-of-the-art deep learning model for motion estimation has also been developed by Hui and colleagues.²¹ It is important to note that the reproduction of a deep learning model from

estimator programs is not significantly different from measuring investigations using the PIV image processing method. Furthermore, an artificial intelligence model has been employed in dentistry to support the clinical decision-making process in certain disciplines²² such as radiology,^{23–25} endodontics,²⁶ and surgery.²⁷

A few studies have been conducted on the hydrodynamic response of EndoActivator tip during the irrigation solution agitation but this present study investigates the solution dynamic behavior through the acquisition of real-time data using a transparent glass model of root canal in order to visualize the oscillation amplitude of the EndoActivator tip during solution activation. This is necessary to provide more knowledge on the mechanism underlying the activation behavior of this device in the solution towards improving the outcomes of the root canal treatment.

The main challenge is to develop a deep learning estimator for non-PIV (absence of seeding particles) based on LiteFlowNet²¹ to be applied to a relatively limited area such as a root canal space as a means of producing high-resolution images. The program also has the ability to process a non-particle image pair input to produce a velocity field output with displacement vectors at every pixel.

MATERIALS AND METHODS

A 22-mm polymer noncutting #25, 0.04 (Dentsply) tip was mounted on an EndoActivator hand-piece (Dentsply Tulsa Dental Specialties, Tulsa, OK) set at a high mode of 190 Hz to activate the irrigant. The handpiece was fixed in a holder to ensure the desired position was maintained. It is important to note that all the experiment was conducted by the same operator.

The conditions within a straight root canal were simulated and visualized using a glass model with an artificial canal and pulp cavity that acted as the reservoir. The model was a glass root canal (Kimia Farma, Bandung, West Java, Indonesia) with a canal inner diameter of 0.4 mm at the apex, the crown height of 8 mm, crown diameter of 6 mm, a taper of 0.06, and an overall length of 25 mm. The canal was filled with a solution containing 17% EDTA while the apex of the model was sealed with composite to allow the conditions within the root canal to be simulated. Moreover, the tip of the sonic instrument was inserted into the solution around 6 mm from the interface and activated passively without any filing motion. A single transparent glass model was used to ensure uniformity in the width and size of the root canal.

It is important to restate that the objective of this study is to observe the hydrodynamic response to EndoActivator tip solution activation in the root canal model. The process was recorded using a Phantom Miro 320S high-speed digital imaging system (Wayne, NJ, USA) incorporated with a macro lens capable of producing 25,000 frames per second with 320x240 pixels per image (60 mm, f/2.8; Nikon, Tokyo, Japan). The sample was illuminated by a Fiber-Lite

LMI-6000 LED continuous light source (Dolan-Jenner Industries, Boxborough, MA, USA). (See Supplemental Video S1 <https://youtu.be/kBKsXf-4Nuw>)

The recordings of the hydrodynamic response were analyzed using in-house Particle Image Velocimetry (PIV) software developed by the Aerodynamics Laboratory at Institut Teknologi Bandung (ITB, West Java, Indonesia) to obtain estimation quantitative data images. The software used optical flow with a convolutional neural network for velocity field estimation rather than using the measured experimental PIV settings with tracer particles.

The data from non-PIV experiments were extracted using a deep learning estimator incorporated with the PIV software developed by the Aerodynamics Laboratory at ITB (Bandung, West Java, Indonesia). Moreover, the user disregarded the last NetE level and imposed the LiteFlowNet trained weights to generate a LiteFlowNet version. The flowchart of the stages involved in the data execution process is, therefore, presented in the following Figure 1.

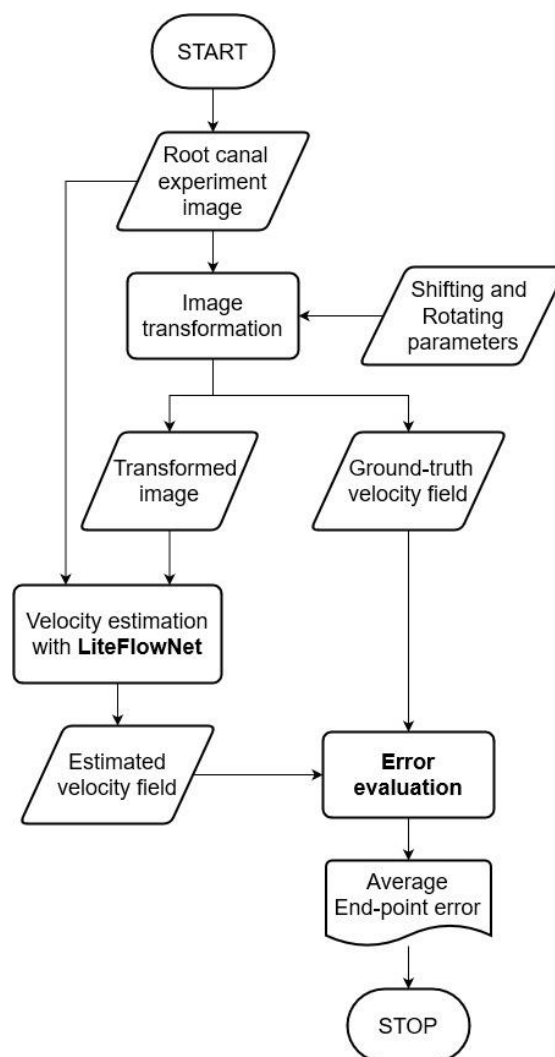


Figure 1. The deep learning motion estimator process in an optically accessible root canal model.

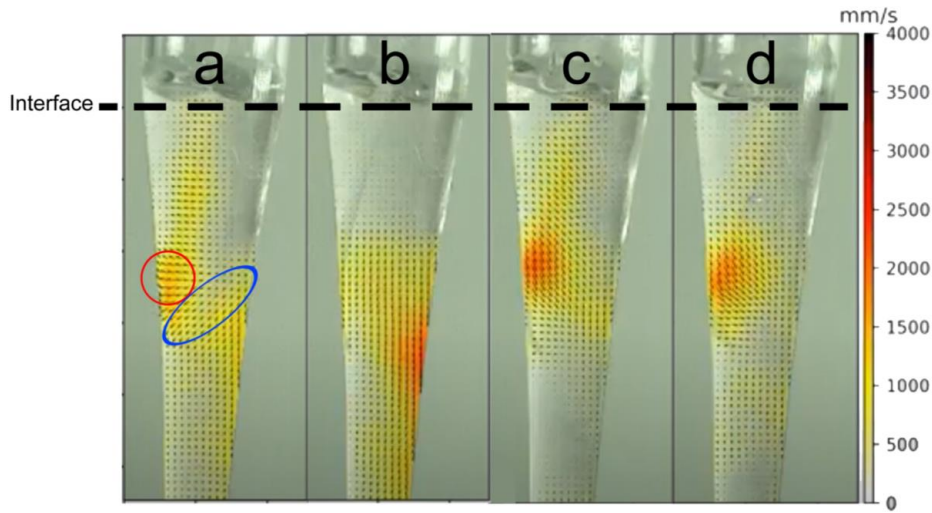


Figure 2. The direction of the flow caused by an EA oscillating tip (indicated by solid arrows). (a) The red circle indicates the flow pattern occasionally occurring perpendicular to the axial of the tip and the oblique flow pattern in blue. Meanwhile, (b) to (d) indicate the visualization of the instantaneous dense velocity fields within the small-scale flow structures near the wall with the orange to a red color indicating the location where a near-wall high-velocity gradient occurred.

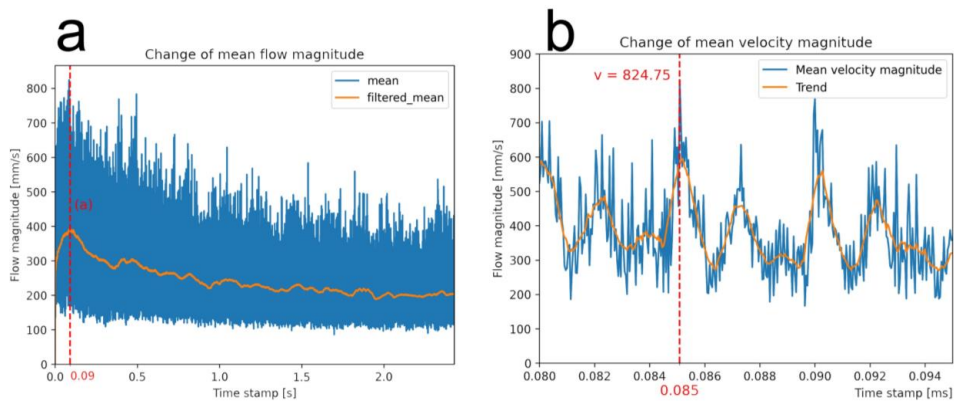


Figure 3. (a) Change of mean flow magnitude as indicated from 0 to a point showing accumulation of energy while the point to 2 sec depicts the decreased fluid flow velocity with the highest recorded at 0.09 sec. (b) The point with the highest magnitude at 824.75 mm/sec.

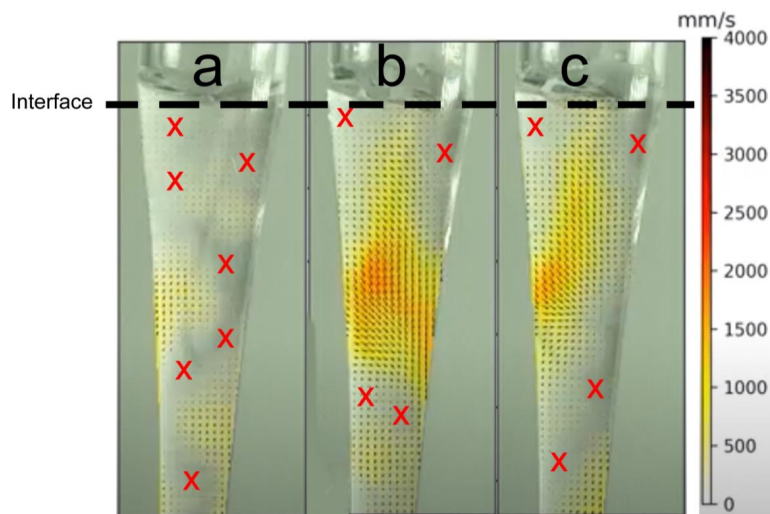


Figure 4. Representative of instantaneous velocity fields with minimum flow magnitude (X).

RESULTS

The results showed that the modified non-enhanced LiteFlowNet program successfully extracted non-particle image pair input to produce velocity field output with displacement vectors in every pixel. The program also provided detailed high-resolution images which enabled smaller scale motion detection while generating a dense motion field for all images and rapidly completing the computer processing.

The flow motion was highly unsteady and this observation was highlighted in this study by focusing only on a limited portion of the canal which was located around the distal end of the tip to enable velocity field visualization. Moreover, the flow patterns perpendicular to the axial flow along the canal (red) and oblique flow patterns (blue) were periodically observed as indicated in Figure 2a. The instantaneous image contained in Figure 2 (b-d) also shows the flow pattern of the solution near the distal end of the tip where the highest amplitude occurs. Furthermore, a periodic flow pattern was discovered at the velocity gradients recorded near the wall during activation. The findings also showed that the velocity fields within this region indicated in red were approximately three to six times higher than those in the surrounding area. The length of the arrows also indicates the magnitude of the velocity while bubbles were generated during activation.

DISCUSSION

Human dentin structure makes it impossible to have a direct visualization of the root canal process and this is the reason in vitro models are usually made of transparent glass but previous studies showed that this method cannot reflect the actual activities in clinical settings. However, it is interesting to know how the fluid behavior and velocity field generation can be visualized in real-time. The experiment conducted showed that the EA tip activation process in the root canal model is in two stages which include the energy accumulation and bubbles regime stages.

The energy accumulation stage: The vibrating EA tip transferred its energy to the solution and created waves which, in turn, caused surface waves to form at the interfaces at the 0-0.09 second range as indicated in Figure 3a. Moreover, the kinetic energy increased to the point that it was sufficiently high to disrupt the air-solution interface with an average fluid magnitude close to 824.75 mm/sec when the amplitude reached its peak (see Supplemental Video S2 <https://youtu.be/6L24NueCIy0>). The highest peak of energy accumulation occurred at 0.085 second as shown in Figure 3b where the bubble started to form for the first time. However, this point is not its natural frequency even though the amplitude of the EA tip seems to reach its peak depending on the frequency applied. Therefore, the fluid flow was unable to reach its maximum needed

to affect the cleaning mechanism. A pilot study was also conducted for confirmation and it showed that the EA tip did not separate when it was being forced to vibrate in the air at its applied frequency. This implies the EA tip did not achieve its resonant or natural frequency which can cause damage or tip separation due to excessive vibration at a higher frequency.²⁸

Bubbles regime stage: This stage lasted between approximately 0.09 and 2 seconds as indicated in Figure 3a and the velocity was observed to reduce gradually to its lowest level reaching a constant speed of approximately 230 mm/sec during bubble formation as indicated in Figure 3a and the near-wall velocity gradients were discovered not to occur. This phenomenon led to the recommendation of continuous replenishment of irrigation solution during activation to reduce the prolonged bubble regime (see Supplemental Video S3 <https://youtu.be/HyXaspb-zZk>).

The up and down flow patterns were observed to hardly form during EA activation in these stages and this can lead to the development of a push-pull mechanism that enhances the removal of smear layer and debris.^{18,29} Furthermore, it was very obvious during the activation that there were lots of areas where the velocity field had the lowest flow magnitude as indicated in Figure 4. This implies the fluid flow was very limited in such areas, thereby, leading to minimal cleaning action and this was assumed to be due to the natural mode shape of the tip. This phenomena is in line with the study conducted by Peeters et al.³⁰ Moreover, the node at the attachment and the antinode at the end of the tip vibrated freely as a cantilever beam model through a back-and-forth linear movement. This oscillation of the EA tip produced a near-wall high-velocity gradient which is proportional to wall-shear stresses but this was observed to be a rare occurrence. It is important to note that the areas of significant changes in the velocity over a short distance are indicated in red as presented in Figure 2. Furthermore, a near-wall high-velocity gradient and the bulk transports of solution are, potentially, the most important variables of the cleaning process within the root canal during activation from a fluid dynamic perspective.¹⁸ It was also observed from the experiment that high gradient velocity on the wall largely occurred more apically around the lower end of the tip and periodically in the same area and represented in red as indicated in Figure 2. Therefore, it is recommended based on the data relating to these stages that the tip should be moved up and down in order to distribute the shear stresses evenly along the canal while the pumping action of the tip induces additional shear stresses on the wall.

These results simply showed that the proposed LiteFlowNet-supported motion estimation program was able to conduct detailed flow estimation of a non-PIV experiment and extract dense velocity fields. Therefore, it is recommended that the tip should be moved up and down and continuous irrigation should be applied during EA activation. There is enormous potential for the development of related topics and this model facilitates further similar research in dentistry.

ACKNOWLEDGMENTS

The authors deny any conflict of interest related to this study and appreciate Professor Zainal Abidin PhD at the Institut Teknologi Bandung (Bandung, Indonesia), Mr. Wowo Watumas at the Phantom Company for providing helpful contributions to this study.

REFERENCES

- Moreno JO, Alves FRF, Gonçalves LS, Martinez AM, Rôças IN, Siqueira JF. Periradicular status and quality of root canal fillings and coronal restorations in an urban Colombian population. *J Endod.* 2013; 39(5): 600–4.
- Gazzaneo I, Vieira GCS, Pérez AR, Alves FRF, Gonçalves LS, Mdala I, Siqueira JF, Rôças IN. Root canal disinfection by single- and multiple-instrument systems: Effects of sodium hypochlorite volume, concentration, and retention time. *J Endod.* 2019; 45(6): 736–41.
- Souza MA, Corralo DJ, Gabrielli ES, Figueiredo JAP, Cohen S, Wolff M, Steier L. Oral bacterial decontamination using an innovative prototype for photocatalytic disinfection. *Clin Oral Investig.* 2022; 26(3): 3005–10.
- Zhang D, Shen Y, de la Fuente-Núñez C, Haapasalo M. In vitro evaluation by quantitative real-time PCR and culturing of the effectiveness of disinfection of multispecies biofilms in root canals by two irrigation systems. *Clin Oral Investig.* 2019; 23(2): 913–20.
- Boutsioukis C, Kastrinakis E, Lambrianidis T, Verhaagen B, Versluis M, van der Sluis LWM. Formation and removal of apical vapor lock during syringe irrigation: a combined experimental and computational fluid dynamics approach. *Int Endod J.* 2014; 47(2): 191–201.
- Loroño G, Zaldivar JR, Arias A, Cisneros R, Dorado S, Jimenez-Octavio JR. Positive and negative pressure irrigation in oval root canals with apical ramifications: a computational fluid dynamics evaluation in micro-CT scanned real teeth. *Int Endod J.* 2020; 53(5): 671–9.
- Boutsioukis C, Verhaagen B, Versluis M, Kastrinakis E, van der Sluis LWM. Irrigant flow in the root canal: experimental validation of an unsteady computational fluid dynamics model using high-speed imaging. *Int Endod J.* 2010; 43(5): 393–403.
- Chen JE, Nurbakhsh B, Layton G, Bussmann M, Kishen A. Irrigation dynamics associated with positive pressure, apical negative pressure and passive ultrasonic irrigations: a computational fluid dynamics analysis. *Aust Endod J.* 2014; 40(2): 54–60.
- Layton G, Wu W-I, Selvaganapathy PR, Friedman S, Kishen A. Fluid dynamics and biofilm removal generated by syringe-delivered and 2 ultrasonic-assisted irrigation methods: a novel experimental approach. *J Endod.* 2015; 41(6): 884–9.
- Macedo R, Verhaagen B, Rivas DF, Versluis M, Wesselink P, van der Sluis L. Cavitation measurement during sonic and ultrasonic activated irrigation. *J Endod.* 2014; 40(4): 580–3.
- Arslan H, Akcay M, Capar ID, Ertas H, Ok E, Uysal B. Efficacy of needle irrigation, EndoActivator, and photon-initiated photoacoustic streaming technique on removal of double and triple antibiotic pastes. *J Endod.* 2014; 40(9): 1439–42.
- Güven Y, Ali A, Arslan H. Efficiency of Endosonic Blue, Eddy, Ultra X and Endoactivator in the removal of calcium hydroxide paste from root canals. *Aust Endod J.* 2022; 48(1): 32–6.
- Marques-da-Silva B, Alberton CS, Tomazinho FSF, Gabardo MCL, Duarte MAH, Vivan RR, Baratto-Filho F. Effectiveness of five instruments when removing calcium hydroxide paste from simulated internal root resorption cavities in extracted maxillary central incisors. *Int Endod J.* 2020; 53(3): 366–75.
- Swimberghe RCD, De Clercq A, De Moor RJG, Meire MA. Efficacy of sonically, ultrasonically and laser-activated irrigation in removing a biofilm-mimicking hydrogel from an isthmus model. *Int Endod J.* 2019; 52(4): 515–23.
- Jensen SA, Walker TL, Hutter JW, Nicoll BK. Comparison of the cleaning efficacy of passive sonic activation and passive ultrasonic activation after hand instrumentation in molar root canals. *J Endod.* 1999; 25(11): 735–8.
- Jiang L-M, Verhaagen B, Versluis M, van der Sluis LWM. Evaluation of a sonic device designed to activate irrigant in the root canal. *J Endod.* 2010; 36(1): 143–6.
- Koch JD, Smith NA, Garces D, Gao L, Olsen FK. In vitro particle image velocity measurements in a model root canal: flow around a polymer rotary finishing file. *J Endod.* 2014; 40(3): 412–6.
- Koch JD, Jaramillo DE, DiVito E, Peters OA. Irrigant flow during photon-induced photoacoustic streaming (PIPS) using particle image velocimetry (PIV). *Clin Oral Investig.* 2016; 20(2): 381–6.
- Robinson JP, Macedo RG, Verhaagen B, Versluis M, Cooper PR, van der Sluis LWM, Walmsley AD. Cleaning lateral morphological features of the root canal: the role of streaming and cavitation. *Int Endod J.* 2018; 51(Suppl 1): e55–64.
- Le Cun Y, Matan O, Boser B, Denker JS, Henderson D, Howard RE, Hubbard W, Jacket LD, Baird HS. Handwritten zip code recognition with multilayer networks. In: *Proceedings 10th International Conference on Pattern Recognition.* Atlantic City, NJ, USA: IEEE Comput. Soc. Press; 1990. p. 35–40.
- Hui T-W, Tang X, Loy CC. LiteFlowNet: A lightweight convolutional neural network for optical flow estimation. In: *IEEE/CVF Conference on Computer Vision and Pattern Recognition.* Salt Lake City, UT, USA: IEEE; 2018. p. 8981–9.
- Shan T, Tay FR, Gu L. Application of artificial intelligence in dentistry. *J Dent Res.* 2021; 100(3): 232–44.
- Orhan K, Bayrakdar IS, Ezhov M, Kravtsov A, Özyürek T. Evaluation of artificial intelligence for detecting periapical pathosis on cone-beam computed tomography scans. *Int Endod J.* 2020; 53(5): 680–9.
- Zheng Z, Yan H, Setzer FC, Shi KJ, Mupparapu M, Li J. Anatomically Constrained Deep Learning for Automating Dental CBCT Segmentation and Lesion Detection. *IEEE Trans Autom Sci Eng.* 2021; 18(2): 603–14.
- Hiraiwa T, Arijji Y, Fukuda M, Kise Y, Nakata K, Katsumata A, Fujita H, Arijji E. A deep-learning artificial intelligence system for assessment of root morphology of the mandibular first molar on panoramic radiography. *Dentomaxillofacial Radiol.* 2019; 48(3): 20180218.
- Aminoshariae A, Kulild J, Nagendrababu V. Artificial intelligence in endodontics: current applications and future directions. *J Endod.* 2021; 47(9): 1352–7.
- Murphy M, Killen C, Burnham R, Sarvari F, Wu K, Brown N. Artificial intelligence accurately identifies total hip arthroplasty implants: a tool for revision surgery. *Hip Int.* 2021; : 1120700020987526.
- Thomson WT. *Theory of vibration with applications.* 4th ed. London: CRC Press; 2018. p. 558.
- Jiang L-M, Verhaagen B, Versluis M, van der Sluis LWM. Influence of the oscillation direction of an ultrasonic file on the cleaning efficacy of passive ultrasonic irrigation. *J Endod.* 2010; 36(8): 1372–6.
- Peeters HH, Silitonga F, Zuhail L. Application of artificial intelligence in a visual-based fluid motion estimator surrounding a vibrating EDDY® tip. *G Ital Endod.* 2022; 35.